DISEASES AND DISORDERS

Microglia morphology and proinflammatory signaling in the nucleus accumbens during nicotine withdrawal

Adewale Adeluyi[1], Lindsey Guerin[1], Miranda L. Fisher[1,2], Ashley Galloway[3], Robert D. Cole[3,4], Sherine S. L. Chan[5,6], Michael D. Wyatt[1], Shannon W. Davis[7], Linnea R. Freeman[8], Pavel I. Ortinski[3,4], Jill R. Turner[1,2]*

Smoking is the largest preventable cause of death and disease in the United States. However, <5% of quit attempts are successful, underscoring the urgent need for novel therapeutics. Microglia are one untapped therapeutic target. While previous studies have shown that microglia mediate both inflammatory responses in the brain and brain plasticity, little is known regarding their role in nicotine dependence and withdrawal phenotypes. Here, we examined microglial changes in the striatum—a mesolimbic region implicated in the rewarding effects of drugs and the affective disruptions occurring during withdrawal. We show that both nicotine and withdrawal induce microglial morphological changes; however, proinflammatory effects and anxiogenic behaviors were observed only during nicotine withdrawal. Pharmacological microglial depletion during withdrawal prevented these effects. These results define differential effects of nicotine and withdrawal on inflammatory signaling in the brain, laying the groundwork for development of future smoking cessation therapeutics.

INTRODUCTION

While smoking cessation substantially reduces the risk of smoking-related diseases such as cancer, stroke, and respiratory and heart diseases (*1*, *2*), nearly 80% of smokers attempting to quit still fail (*3*). Currently, tobacco smoking is the leading cause of preventable morbidity and mortality globally (*4*), which underscores the need for better therapeutics for nicotine dependence. Pharmacotherapies for nicotine dependence have largely targeted nicotinic acetylcholine receptors (nAChRs), which are expressed primarily on neurons, as activation of these receptors by nicotine mediates the rewarding effects of tobacco (*3*, *5*–*7*). However, the molecular mechanism underlying vulnerability to smoking relapse is multifaceted (*3*). One avenue for development of new therapeutics is expanding investigations to examination of the potential involvement of non-neuronal cell types such as microglia, which are increasingly emerging as active players in brain health and disease.

Microglia are highly specialized resident immune cells, which act as the brain's homeostatic sensor. Their constant surveillance of the brain microenvironment enables them to detect and respond to homeostatic perturbations by altering their own morphology in diverse ways depending on the type of stimuli they sense. Such changes in microglial morphology are more indicative of an imbalance in CNS homeostasis following an insult or injury and not a particular activation phenotype (M1 proinflammatory phenotype or M2 anti-inflammatory phenotype) as initially conceptualized (*8*). Furthermore, studies have described microglia as critical elements in synaptic remodeling (*9*, *10*), as well as learning and memory (*11*)—processes prominently affected during development of drug dependence (*12*, *13*). In addition to neuroplasticity-related events, microglia actively participate in reactive oxygen species (ROS) generation (*14*). While ROS are key intracellular signaling molecules for normal cell function, they can become toxic when there is a chronic imbalance between oxidant and antioxidant signaling within the cell, termed oxidative stress (*15*). Since neurons are particularly susceptible to oxidative insult, aberrant ROS production and signaling can significantly affect brain function and behavior (*16*, *17*). For example, correlative studies examining patients diagnosed with Parkinson's disease found a strong relationship between oxidative stress and striatal neurodegeneration (*18*). However, while the striatal neurocircuit is a major site for neuroadaptive events underlying addictive processes (*19*), the effects of nicotine withdrawal on microglial phenotype and ROS homeostasis in this region are unknown.

The striatum is a heterogeneous structure with two distinct subregions—the caudate putamen, which contributes to motor functions and movement, and the nucleus accumbens, which is key for motivation and reward processes (*19*). Our laboratory (*20*, *21*) and others (*22*) have shown that anxiety is a discrete, quantifiable symptom of nicotine withdrawal, which has been shown to directly affect smoking relapse in humans (*23*). Previous studies in humans have demonstrated the contribution of mesolimbic dopamine signaling in the nucleus accumbens to anxiety-related processes (*24*, *25*). Further, chronic stress studies have reported increased levels of oxidative stress markers in other parts of the mesolimbic circuitry to coincide with increased anxiety-like behavior (*26*, *27*). However, it is unknown whether nicotine withdrawal elicits changes in microglial morphology and function, and whether these changes directly affect anxiety. Our studies report nucleus accumbens–specific alterations in microglial morphology and ROS homeostasis. Further, we demonstrate compelling evidence that microglia are critical mediators of anxiety-like behaviors in mice during nicotine withdrawal.

RESULTS

Chronic nicotine and withdrawal alter microglial morphology in the nucleus accumbens

Morphological changes and release of proinflammatory cytokines are canonical features of activated microglia (*28*). To evaluate both

[1]Department of Drug Discovery and Biomedical Sciences, University of South Carolina, Columbia, SC, USA. [2]Department of Pharmaceutical Sciences, University of Kentucky College of Pharmacy, Lexington, KY, USA. [3]Department of Pharmacology, Physiology, and Neuroscience, University of South Carolina School of Medicine, Columbia, SC, USA. [4]Department of Neuroscience, University of Kentucky School of Medicine, Lexington, KY, USA. [5]Department of Drug Discovery and Biomedical Sciences, Medical University of South Carolina, Charleston, SC, USA. [6]Neuroene Therapeutics, Mt Pleasant, SC, USA. [7]Department of Biology, Furman University, Greenville, SC, USA. [8]Department of Biological Sciences, University of South Carolina, Columbia, SC, USA.
*Corresponding author. Email: jill.turner@uky.edu

features during chronic nicotine and withdrawal, mice were administered saline or nicotine (18 mg kg^{-1} day^{-1}) via osmotic minipump implantation, and at 2 weeks, a 48-h withdrawal was initiated by removal of implanted pumps in mice earmarked for nicotine withdrawal and their saline controls (Fig. 1A). Striatal tissues from mice receiving chronic saline and nicotine or undergoing 48-hour withdrawal from chronic nicotine (WD) showed subregional differences in microglial morphological changes. In the nucleus accumbens, both nicotine-treated and WD-treated mice possessed microglia with a larger cell area and a larger cell perimeter, but not with a longer process length compared to their saline counterparts. This pattern contrasts with that in the caudate putamen, which displayed an increase only in microglial process length during 48-hour WD (Fig. 1, B and C, i to iii). Next, we evaluated mRNA expression levels of tumor necrosis factor–α (TNFα) and interleukin-1β (IL-1β)—proinflammatory cytokines often linked with microglia activation. These results demonstrate a differential mRNA profile of these cytokines in chronic nicotine and withdrawal mice. In the nucleus accumbens, TNFα and IL-1β mRNA levels were elevated in the nicotine withdrawal mice compared to chronic saline and nicotine counterparts, suggesting a muted proinflammatory response during chronic nicotine treatment. In contrast, in the caudate putamen, there was a significant decrease in IL-1β mRNA expression, but no significant change in TNFα mRNA expression between treatment groups (Fig. 1, D and E). Taken together, these results demonstrate that while both chronic nicotine and withdrawal alter microglial morphology indicative of activation in the nucleus accumbens, they induce differential microglial inflammatory responses, suggesting that distinct microglial phenotypes are elicited by chronic nicotine and withdrawal from chronic nicotine.

Nicotine withdrawal induces ROS in the nucleus accumbens

Given that excessive production of ROS is often associated with microglial activation (*29*), we directly examined ROS generation in the nucleus accumbens and caudate putamen of saline, chronic nicotine,

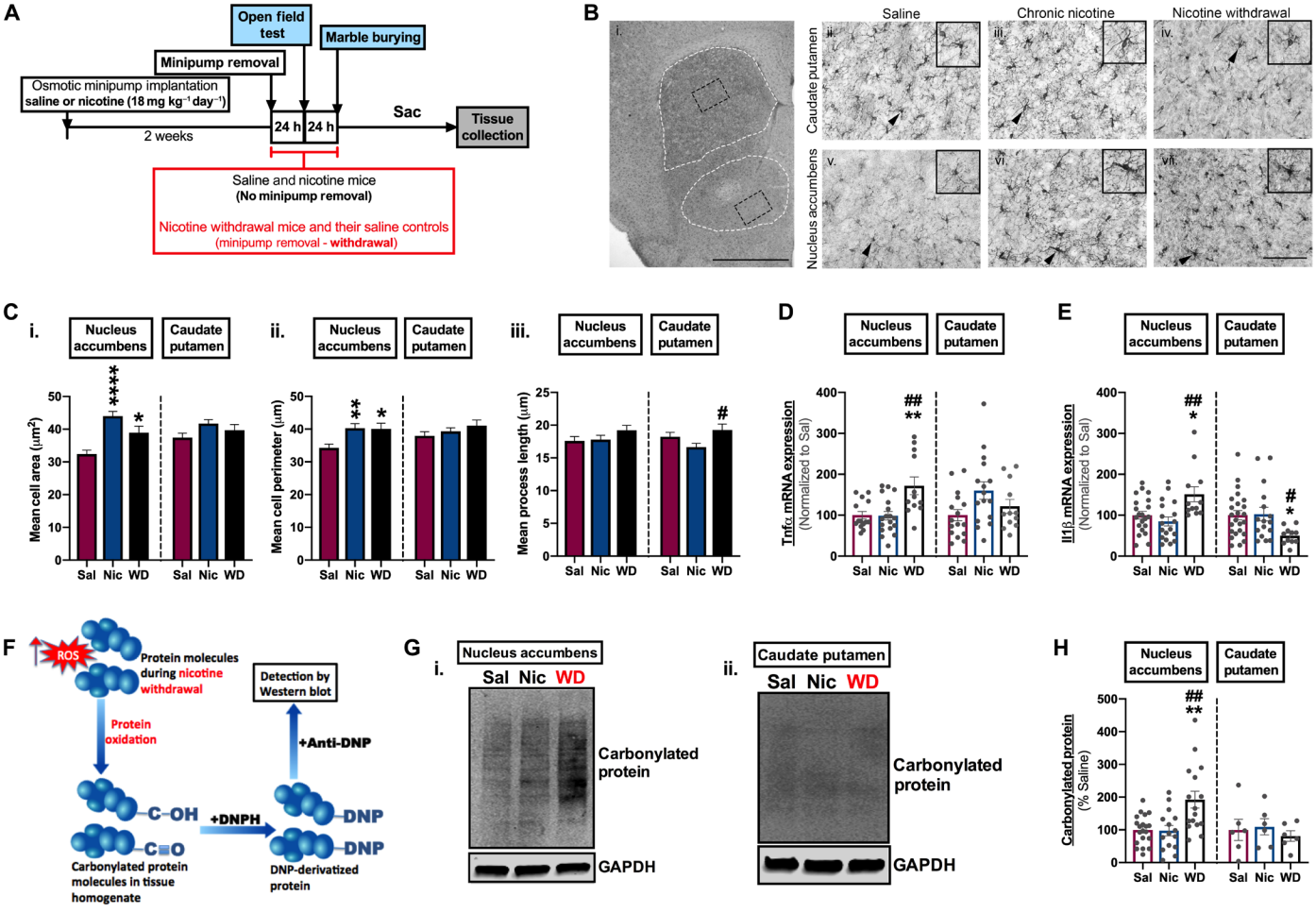

Fig. 1. Nicotine withdrawal alters microglial morphology and induces reactive oxygen species in the nucleus accumbens. (**A**) Experimental design. (**B**) Representative images of IBA1-positive microglia. (i) White dotted traces delineate the caudate putamen (dorsal) and nucleus accumbens (ventral); black dotted traces indicate the area where (ii) to (vii) were taken. Scale bar, 1 mm. Caudate putamen of (ii) saline (Sal) mice, (iii) nicotine (Nic) mice, and (iv) nicotine withdrawal (WD) mice. Nucleus accumbens of (v) Sal mice, (vi) Nic mice, and (vii) WD mice. Scale bar, 100 μm. (C) Quantitation of (B, ii to vii). (i) Cell area (soma size), (ii) cell perimeter, and (iii) process length. Bar charts showing expression of (D) TNFα mRNA and (E) IL-1β mRNA in the nucleus accumbens and caudate putamen. (F) Schematics showing mechanism of reactive oxygen species detection by protein carbonylation assay (protein and arrow icons were downloaded from Reactome (*31*). (G) Representative immunoblot showing carbonylated protein levels: (i) nucleus accumbens and (ii) caudate putamen. (H) Quantitation of (G). [Compared to Sal—$^{*}P < 0.05$, $^{**}P < 0.01$, $^{****}P < 0.0001$; compared to Nic—$^{\#}P < 0.05$, $^{\#\#}P < 0.01$; (C) n = minimum of 116 cells were quantified from four to eight animals per treatment group; (D and E) n = 12 to 24 per treatment group; (H) n = 6 to 19 per treatment group.]

and nicotine withdrawal mice using a protein carbonylation assay. Carbonylated proteins are well-established markers for oxidative stress because they are representative products of protein oxidation, which occurs either by direct or by indirect reaction of a protein with ROS or secondary by-products of oxidative stress (*30*) [Fig. 1F; protein and arrow icons were downloaded from Reactome (*31*)]. Similar to our previous observations of TNFα and IL-1β mRNA levels, we found that nicotine withdrawal animals had increased levels of carbonylated proteins in the nucleus accumbens compared to the chronic saline and nicotine equivalents, while there were no changes between treatment groups in the caudate putamen (Fig. 1, G and H). These data further reinforce that chronic nicotine and withdrawal from chronic nicotine result in dissimilar inflammatory responses and that these effects within the striatum are specific to the nucleus accumbens.

Nicotine withdrawal induces anxiogenic behavior in mice

Anxiety is a key affective nicotine withdrawal symptom, which is associated with nucleus accumbal function (*25*). Therefore, we evaluated this behavior given our findings showing nucleus accumbens–specific changes in microglial morphology and ROS homeostasis. We used two well-validated behavioral models of anxiety, the marble-burying (MB) test and the open field (OF) test. These behavioral tests were conducted at 24-hour (OF test) and 48-hour (MB test) withdrawal time points (Fig. 1A). In the MB test, nicotine withdrawal animals buried more marbles than their chronic nicotine and saline counterparts (Fig. 2A), indicative of an anxiogenic effect during nicotine withdrawal. Similarly, in the OF test, our results show that nicotine withdrawal animals spent less time in the center of the arena compared to their saline and chronic nicotine equivalents, which is also an indicator of anxiogenic effects (Fig. 2, B and D). Further analyses show that these effects were not due to alterations in locomotor activity, as there were no differences in distance traveled between any of the treatment groups (Fig. 2C).

Microglia-enriched NADPH oxidase 2 is increased in the nucleus accumbens during nicotine withdrawal

Among the many molecular mechanisms of intracellular ROS generation (*32*), the NADPH oxidase (Nox) system is a major source of intracellular ROS production in the brain (*33*). In fact, interplay between Nox, ROS, and TNFα is reported to be critical in the development of many inflammatory diseases (*34*–*36*). Because we observed that nicotine withdrawal increases both ROS and TNFα expression in the nucleus accumbens, we next examined the nucleus accumbens for changes in the primary Nox isoforms expressed in the brain (Nox1, Nox2, and Nox4). Quantitative polymerase chain reaction (qPCR) analysis of Nox1 and Nox4 in the nucleus accumbens showed no significant differences between treatment groups. However, qPCR analyses of Nox2 showed a significant increase in Nox2 expression in the nucleus accumbens of nicotine withdrawal mice compared to their saline and chronic nicotine equivalents (Fig. 3A, i to iii). Furthermore, no significant differences in Nox2 mRNA expression were observed in the caudate putamen (Fig. 3B), again reinforcing subregional differences in the striatum in response to nicotine withdrawal. Together, these data support the premise that increased nucleus accumbal Nox2 during nicotine withdrawal may contribute significantly to ROS

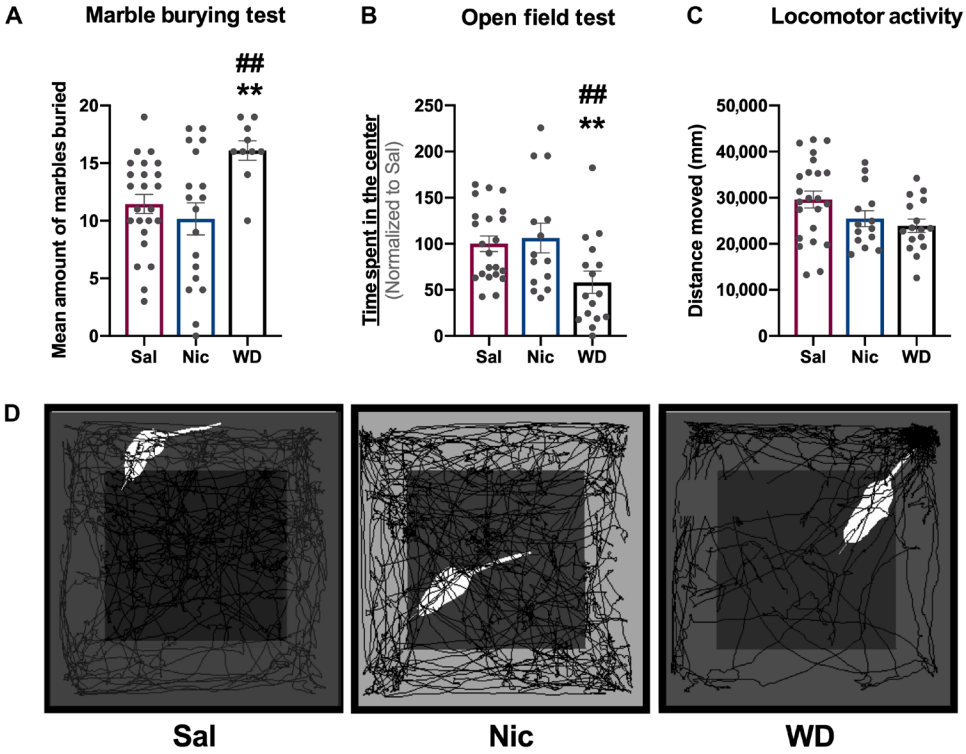

Fig. 2. Nicotine withdrawal induces anxiety-like phenotype in mice. (**A**) MB test: Bar graph showing the mean value of marbles buried by Sal, Nic, and WD mice. (**B**) OF test: Bar chart showing the time spent in the center of the OF arena by Sal, Nic, and WD mice. (**C**) Locomotor activity: Bar chart showing the average distance moved in the OF arena by Sal, Nic, and WD mice. (**D**) Representative OF traces of Sal, Nic, and WD mice. [Compared to Sal—$^{**}q < 0.01$; compared to Nic—$^{\#\#}q < 0.01$; (A to C) $n = 9$ to 23 per treatment group.]

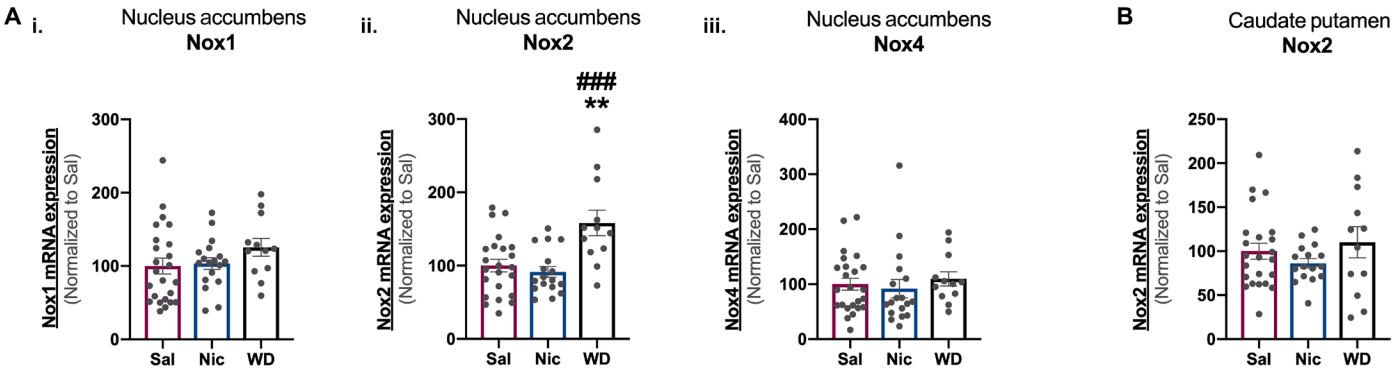

Fig. 3. Nicotine withdrawal increases Nox2 expression in the nucleus accumbens. (**A**) Bar graph showing qPCR analysis of Nox isoforms (primarily expressed in the brain) in the nucleus accumbens of Sal, Nic, and WD mice. (i) Nox1, (ii) Nox2, and (iii) Nox4. (**B**) Bar graph showing qPCR analysis of Nox2 mRNA expression in the caudate putamen of Sal, Nic, and WD mice. [Compared to Sal—$^{**}P < 0.01$; compared to Nic—$^{###}P < 0.001$; (A and B) $n = 12$ to 24 per treatment group.]

production in this region and potentially affect nicotine withdrawal–related anxiety. Previous studies have shown that Nox2 is primarily expressed in microglia and they are the major source of ROS in the brain (*37*). However, given that these studies investigating Nox expression in brain cell types induced Nox with lipopolysaccharide or examined Nox in pathological states (*38*), we evaluated nucleus accumbal tissues from adult, naïve mice for relative enrichment of specific Nox isoforms in neuronal and glial cell types. To do this, we used magnetic-activated cell sorting (MACS) for isolation and purification of cell types in nucleus accumbal tissues. Validation of our approach shows that isolated microglia were highly enriched for $CD11b^+$, Tmem119, and P2ry12 compared to total homogenate or other isolated cell types (Fig. 4A, i to iii). We next examined these samples for Nox subtype enrichment. While Nox1 and Nox4 mRNA analyses showed significant enrichment in the liver compared to total homogenate, there were no significant differences between total homogenate and the evaluated brain cell types (Fig. 4B, i and ii). In contrast, Nox2 mRNA is significantly enriched in both microglia and liver compared to total homogenate, astrocytes, neurons, and oligodendrocytes (Fig. 4B, iii). These data support the idea that Nox2 is highly expressed in microglia in the nucleus accumbens, which may underpin the increased ROS generation observed in the nucleus accumbens during nicotine withdrawal.

Microglial depletion blocks increases in Nox 2 expression and ROS in the nucleus accumbens and attenuates nicotine withdrawal–related anxiety

We show that withdrawal from chronic nicotine treatment, but not chronic nicotine treatment itself, elicits proinflammatory microglial signaling in the nucleus accumbens. In addition, we demonstrate that Nox2 expression in the nucleus accumbens is restricted to microglia, and alterations in microglial signaling in the nucleus accumbens may contribute to nicotine withdrawal–related anxiety. Therefore, to directly determine the contribution of microglia in these processes, we used PLX5622, a colony-stimulating factor–1 receptor (CSF1R) inhibitor, to pharmacologically deplete microglia in animals undergoing withdrawal from saline or nicotine treatment. To do this, 7 days following initial osmotic minipump implantation, both saline- and nicotine-treated animals were given either control chow or PLX5622 chow. One week later, withdrawal from chronic saline or nicotine was initiated by surgically removing the pumps from all subjects. Saline and nicotine withdrawal–treated animals were then tested in the OF and MB tests at 24- and 48-hour withdrawal time points, respectively (Fig. 5A). We first evaluated the success of our microglial depletion by examining microglial density in the nucleus accumbens. PLX5622-treated animals showed a 70 to 80% reduction in $Iba1^+$ cells/mm^2 in the nucleus accumbens compared to control chow–treated controls (Fig. 5B, i and ii). Similarly, PLX5622-treated animals exhibited significant reductions in mRNA expression of the microglial markers Tmem119 and P2ry12 compared to their controls (Fig. 5C, i and ii). Furthermore, given that CSF1R is also expressed on monocytes, we next examined whether infiltrating monocytes could be contributing to the observed nicotine withdrawal effects by comparing the expression profile of the microglial markers Tmem119 and P2ry12 to a monocyte marker, C-C chemokine receptor 2 (Ccr2), which has been previously described by many studies as a critical element for trafficking and assembly of myeloid cells in the brain (*39*, *40*). Our data demonstrate an extremely low Ccr2 expression level compared to Tmem119 and P2ry12 in all treatment groups (Fig. 5D). Furthermore, the baseline expression of $Ccr2^+$ monocytes in the nucleus accumbens is comparable across treatment groups, regardless of CSF1R inhibition or nicotine treatment (Fig. 5D), suggesting that infiltrating monocytes contribute little to our reported observations during nicotine withdrawal. Next, we examined the impact of microglia depletion on Nox2 expression in the nucleus accumbens during nicotine withdrawal. qPCR analyses showed that Nox2 mRNA expression was again significantly increased in the nucleus accumbens of control chow nicotine withdrawal mice compared to saline controls, irrespective of PLX5622 treatment. This increase in Nox2 mRNA expression during nicotine withdrawal was absent in nicotine withdrawal animals maintained on PLX5622 (Fig. 6A). Next, we evaluated the effect of microglial knockdown on nicotine withdrawal–induced ROS in the nucleus accumbens. Again, we observed a significant increase in protein carbonylation during nicotine withdrawal compared to saline controls, which was absent in PLX5622-treated subjects undergoing nicotine withdrawal (Fig. 6B, i and ii). Finally, we assessed the impact of microglial depletion on anxiety-like behavior as an endophenotype of nicotine withdrawal. In the MB test, control chow nicotine withdrawal mice buried more marbles compared to their saline withdrawal controls. In contrast, no differences were observed in the MB test between the PLX5622 chow nicotine withdrawal mice and their PLX5622 chow saline withdrawal equivalents (Fig. 6C). Similarly, our OF analyses demonstrated that control chow nicotine withdrawal mice spent less time

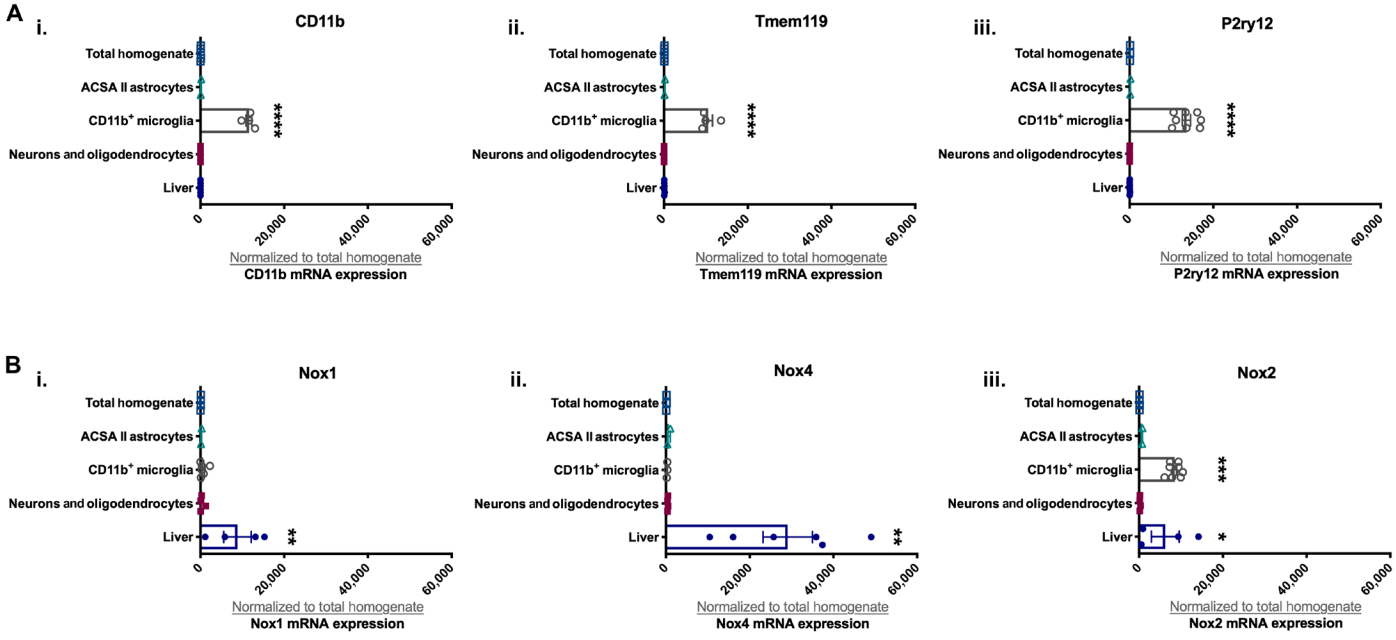

Fig. 4. Nox2 is expressed in microglia. (**A**) Bar graph showing qPCR analysis of microglia markers in the liver, brain cell types, and tissue (total homogenate). (i) CD11b, (ii) Tmem119, and (iii) P2ry12. (B) Bar graph showing qPCR analysis of Nox isoforms in the liver, brain cell types, and tissue. (i) Nox1, (ii) Nox4, and (iii) Nox2. [Compared to total homogenate—$^{*}P < 0.05$, $^{**}P < 0.01$, $^{***}P < 0.001$, $^{****}P < 0.0001$; (A and B) $n = 2$ to 9 per treatment group.]

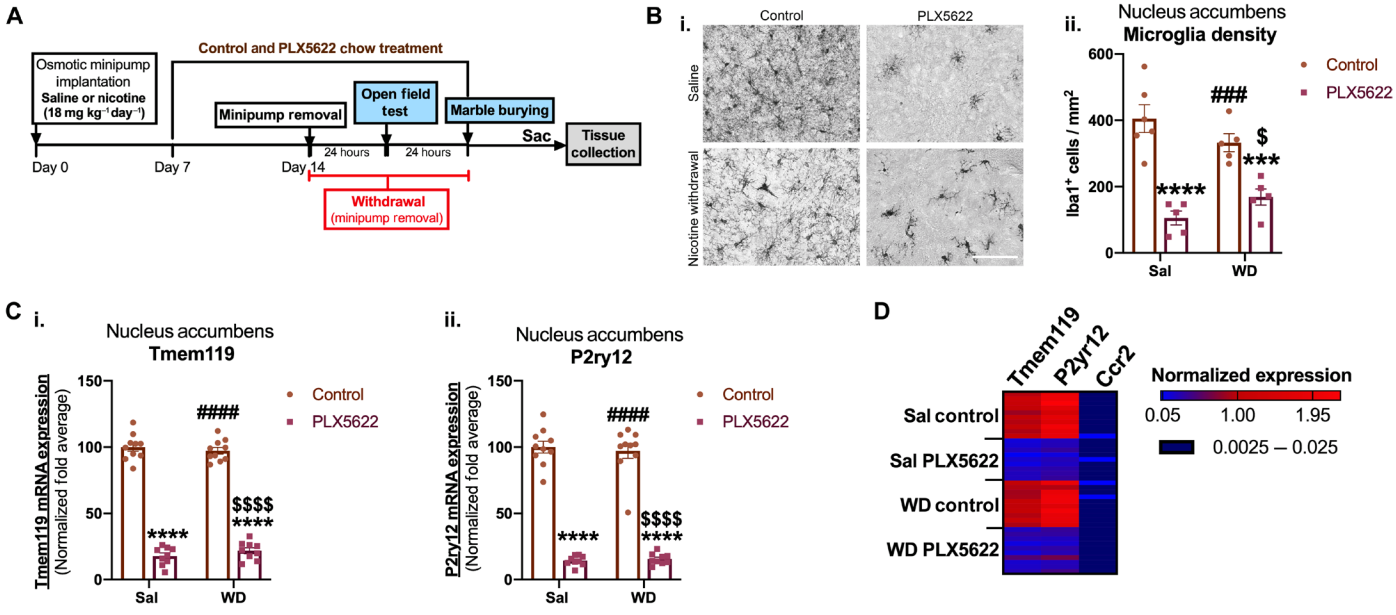

Fig. 5. Inhibition of CSF1R depletes microglia in the nucleus accumbens. (**A**) Experimental design. (**B**) (i) Representative images of IBA1-positive microglia in the nucleus accumbens of control chow and PLX5622 chow Sal, as well as their WD equivalents. (ii) Quantitation of (B, i). (**C**) Bar graph showing qPCR analysis of microglia markers in the nucleus accumbens of control chow and PLX5622 chow Sal, as well as their WD equivalents. (i) Tmem119 and (ii) P2ry12. Heatmap showing normalized expression profile of Tmem119, P2ry12, and Ccr2 in the nucleus accumbens of control chow and PLX5622 chow Sal, as well as their WD equivalents. [Compared to Sal control—$^{***}P < 0.001$, $^{****}P < 0.0001$; compared to Sal PLX5622—$^{\#\#\#}P < 0.001$, $^{\#\#\#\#}P < 0.0001$; compared to WD control—$^{\$}P < 0.05$, $^{\$\$\$\$}P < 0.0001$; (B, ii) $n = 5$ per treatment group; (C and D) $n = 10$ per treatment group.]

in the center of the arena compared to their saline controls, indicating an anxiogenic response. This anxiogenic effect was absent in PLX5622-treated nicotine withdrawal–treated animals (Fig. 6, D and F). These effects were not due to alterations in locomotor activity, as there were no observed differences in distance traveled between animals from any of the treatment groups (Fig. 6E).

DISCUSSION

A recent study in human subjects using [^{11}C]DAA1106, a ligand for translocator protein (TSPO) and a putative indicator of microglial activation, suggested that smokers with nicotine on board have less microglial activation than nonsmokers (*41*). However, mechanistic interpretation of these results was difficult given the nuances regarding

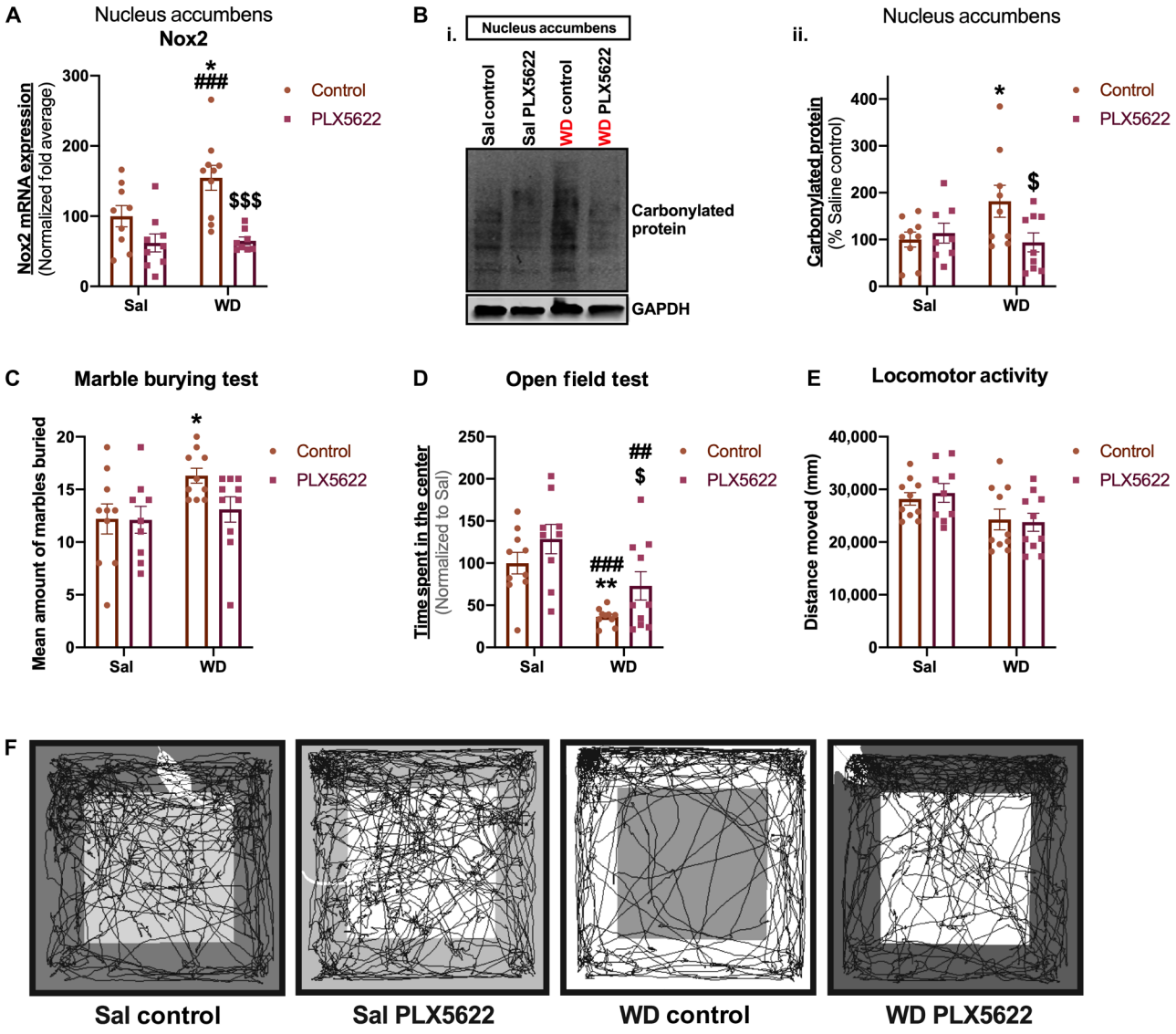

Fig. 6. Microglia depletion attenuates nicotine withdrawal–related anxiety. (**A**) Bar graph showing qPCR analysis of Nox2 in the nucleus accumbens of control chow and PLX5622 chow Sal, as well as their WD equivalents. (**B**) (i) Representative immunoblot showing the expression of carbonylated proteins in the nucleus accumbens of control chow and PLX5622 chow Sal, as well as their WD equivalents. (ii) Quantitation of (B, i). (**C**) MB test: Bar graph showing the mean amount of marbles buried by control chow and PLX5622 chow Sal, as well as their WD equivalents. (**D**) OF test: Bar chart showing the time spent in the center of the OF arena by control chow and PLX5622 chow Sal, as well as their WD equivalents. (**E**) Locomotor activity: Bar chart showing the average distance moved in the OF arena by control chow and PLX5622 chow Sal, as well as their WD equivalents. (**F**) Representative OF traces of control chow and PLX5622 chow Sal, as well as their WD equivalents. [Compared to Sal control—$^{*}P < 0.05$, $^{**}P < 0.01$; compared to Sal PLX5622—$^{\#\#}P < 0.01$, $^{\#\#\#}P < 0.001$; compared to WD control—$^{\$}P < 0.05$, $^{\$\$\$}P < 0.001$; (A, Bii, C, D, and E) $n = 9$ to 10 per treatment group.]

microglial activation. This study distinguishes the direct effects of chronic nicotine on microglial activation compared to the effects of withdrawal from chronic nicotine, thereby significantly contributing to our understanding of microglial dynamics in smokers and how these changes may affect nicotine withdrawal symptoms, such as anxiety. We show that chronic nicotine and withdrawal alter microglial morphological changes but trigger dissimilar inflammatory responses in the nucleus accumbens. Further, we report elevated ROS levels in the nucleus accumbens only during nicotine withdrawal and suggest from our study that Nox2, which is highly enriched in microglia, is the major ROS-producing machinery. However, in contrast to our findings in the nucleus accumbens, we show that neither chronic nicotine nor withdrawal triggers any of these effects in the caudate putamen. To directly demonstrate the necessity of microglia for these effects, we used PLX5622 to deplete microglia in the brain. We show that microglial depletion prevented nicotine withdrawal increases in Nox2 mRNA and ROS in the nucleus accumbens, as well as blunted associated nicotine withdrawal–related anxiety-like behaviors in our model. In total, our experiments support the observations by Brody *et al.* (*41*), showing decreased inflammatory signaling in the brain during chronic nicotine use. However, our study extends these observations to demonstrate a number of key mechanistic findings: (i) while chronic nicotine does not elicit a proinflammatory response in the nucleus accumbens, morphological analysis suggests that microglia are indeed activated in this brain region; (ii) withdrawal from chronic nicotine, such as that experienced by a smoker during

an acute quit attempt (24- to 48-hour WD), elicits a proinflammatory response in the nucleus accumbens, but not the caudate putamen; (iii) the proinflammatory response due to acute nicotine withdrawal encompasses a constellation of molecular effects, including increased Nox2 expression, increased ROS generation, and increased proinflammatory cytokines; and (iv) attenuating microglial contributions to this process via microglial depletion reversed all molecular effects as well as attenuated anxiety-like behavior in our model. Our findings suggest that further investigation is merited to examine inflammatory responses in human smokers during acute withdrawal and suggest that therapeutic development of microglial modulators may be beneficial as smoking cessation aids.

Microglial phenotypes during chronic nicotine and withdrawal in the striatum

Microglia are central players in an increasing number of brain disorders (*8*), and understanding their responsivity and role in nicotine dependence is becoming increasingly urgent. In our model, both chronic nicotine and withdrawal induce activation or remodeling of the highly adaptable resting microglia in the nucleus accumbens, but not in the caudate putamen, suggesting that microglial responsivity to drug cues may be shaped by the specialized role of their local CNS environment. For example, a recent study examining microglia transcriptome across the basal ganglia reported regional heterogeneity of resident microglia and indicated local cues as a critical mediator of microglia phenotype and their diversity (*42*). In addition, this study also showed that genes associated with oxidative signaling and ROS homeostasis are among the top 10 most abundant genes in nucleus accumbal microglia, but not microglia from other parts of the basal ganglia (*42*). This is consistent with our findings that show disruption in ROS homeostasis in the nucleus accumbens, but not the caudate putamen, during nicotine withdrawal. Another important finding is the dissimilar expression of proinflammatory cytokines (TNFα and IL-1β) and ROS in the nucleus accumbens during chronic nicotine and withdrawal. We report an absence of induction of TNFα and IL-1β cytokines during chronic nicotine treatment despite microglial morphological changes, suggesting the absence of a classical proinflammatory response. This observation is in accordance with a study that showed inhibition of proinflammatory cytokines in a lipopolysaccharide-activated primary microglial culture pretreated with nicotine (*43*). In addition, our findings are also in line with clinical studies demonstrating nicotine's neuroprotective properties in neurodegenerative diseases (*44*, *45*) as well as with findings that smokers have reduced inflammatory responses compared to nonsmokers (*41*). However, this is in contrast to nicotine withdrawal, which presents with a distinct proinflammatory profile that is perhaps present selectively in regions with highly implicated nicotine dependence, such as the nucleus accumbens as reported here. One caveat when comparing our findings with those observed in smokers, however, relates to the relative timing of nicotine exposure. In our model, animals were treated with continuous chronic nicotine over a 2-week period. Smokers, in contrast, undergo fluctuating levels of nicotine throughout the 24-hour day, primarily between sleep and wake. However, it should be noted that during normal wake periods, smokers tend to titer their cigarette consumption to achieve a steady level of nicotine (*46*), further complicating this issue. Previous studies in rodents have examined differences between continuous and intermittent nicotine exposure, but their results regarding withdrawal phenotypes in these differing paradigms were inconclusive. For example, Brynildsen *et al.* (*47*) found that continuous treatment of nicotine resulted in less robust somatic nicotine withdrawal behaviors in animals compared to pulsatile delivery at the same doses. In contrast, Semenova *et al.* (*48*) showed that withdrawal from continuous nicotine treatment resulted in more robust withdrawal phenotypes in the intracranial self-stimulation paradigm compared to intermittent nicotine delivery at the same doses. While their methods of inducing withdrawal may differ, these studies underscore the need for future experiments comparing the effects of continuous versus pulsatile delivery of nicotine on withdrawal phenomena, including microglial alterations.

Of note, the few studies available on the role of microglia in drug dependence reported that microglial activation and related proinflammatory effects were directly elicited by the drugs of abuse examined, namely, cocaine (*49*) and morphine (*50*). Similar to our findings, microglial activation and elevated levels of inflammatory signals in those studies were restricted to the nucleus accumbens, but our findings contrast with those earlier studies in that nucleus accumbal inflammatory responses occur only during withdrawal from nicotine and not due to exposure to nicotine itself. In addition to their immune function, microglia are also involved in synaptic function and plasticity; therefore, their alterations within the nucleus accumbens, which is a critical brain circuit for addictive processes, may enhance the development of aberrant synaptic connections and plasticity underlying drug dependency. Together, these data suggest that the synaptic cues specific to the nucleus accumbens during exposure to chronic nicotine or withdrawal from chronic nicotine distinctly influence the phenotype of its resident microglia. Moreover, these findings have the potential to reveal sex-specific effects. While our findings are currently restricted to male mice, future studies assessing these effects in female mice are critically needed, especially given the well-described sex differences observed in microglia-related studies (*51*).

Microglia-related Nox 2 in the nucleus accumbens during nicotine withdrawal

Nox systems are the primary systems implicated in disease-related aberrant ROS production (*52*). Among the Nox isoforms expressed in the brain (Nox1, Nox2, and Nox4 (*53*)), our findings implicate Nox2 as the source of excessive ROS in the nucleus accumbens during nicotine withdrawal. Similar to previous studies (*37*, *38*), we report that Nox2 is enriched in microglia in the nucleus accumbens of adult, naïve mice, suggesting that Nox2 in microglia is the likely source of ROS during nicotine withdrawal. Further, previous studies have shown that lipopolysaccharide stimulation of BV2 microglial cell lines resulted in Nox2-dependent ROS production (*54*). Overall, these results suggest that microglia-derived Nox2 contributes significantly to aberrant ROS levels in the nucleus accumbens during nicotine withdrawal.

Microglial function and anxiety-like behavior during nicotine withdrawal

Several studies have implicated microglial function in anxiety-related disorders (*55*, *56*); however, the role of microglia in nicotine withdrawal–related anxiety is unknown. Our study demonstrates that depletion of microglia during nicotine withdrawal prevented the associated increases in Nox2 mRNA and ROS levels in the nucleus accumbens, as well as the concordant anxiety-like behaviors observed during nicotine withdrawal. We found in our experiments that despite strong

microglial suppression in PLX5622 chow saline mice and their withdrawal equivalents, we observed no behavioral effects of this manipulation compared to saline-treated mice maintained on control chow. This suggests that microglial knockdown alone is insufficient to affect these behaviors in the absence of nicotine withdrawal and that it is the nicotine withdrawal–induced microglial signaling underlying nicotine withdrawal–related anxiety. These findings provide a strong link between microglial function and nicotine withdrawal–related anxiety and suggest a direct contribution of microglial-related Nox2 and associated aberrant ROS production in the nucleus accumbens to the development of anxiogenic behavior during nicotine withdrawal.

Because there is no single behavioral model of anxiety that measures all aspects of anxiety, in our study, we used two models of anxiety to cross-validate our experimental outcomes. However, while both behavioral paradigms are well known and validated measures of anxiety-like behavior that are sensitive to clinically used anti-anxiety medications such as benzodiazepines and antidepressants (*57*, *58*), future studies using tasks with high face validity to clinically used measures of negative valence and uncertainty, such as novelty-induced hypophagia test (a measure of response to potential harm), could further these results. In addition, withdrawal from nicotine leads to a diverse array of clinical symptoms, spanning cognitive, affective, and motivational domains. A recent study using a model of precipitated nicotine withdrawal showed that elements of cognitive disruption in this model correlate with microglial activation in the hippocampus and prefrontal cortex (*59*). However, it is important to note that mecamylamine, which is used in the precipitated withdrawal model, has cognitive-depressive effects on its own in rodents (*60*), monkeys (*61*), and even humans (*62*). Further complicating interpretation of these results, the direct effects of this nicotinic antagonist on microglia in the absence of nicotine is unknown. However, these results in tandem with our own suggest that further examination of microglial contributions to diverse nicotine withdrawal symptoms is warranted.

Perspectives on future smoking cessation pharmacotherapies

Currently, there are three Food and Drug Administration–approved pharmacotherapies for smoking cessation: varenicline (a nicotinic selective partial agonist), bupropion (a norepinephrine-dopamine reuptake inhibitor), and nicotine replacement therapy (NRT, such as patch, gum, etc.). While each of these therapeutics has quantifiable success as smoking cessation aids, the best-in-class medication, varenicline, results in only 40% abstinence success at 12 weeks and less than 20% at 1 year post-quit (*63*). This underscores the urgent need for new drug targets in the development of new smoking cessation aids. In this study, we outline a series of novel findings implicating neuroinflammatory responses in the etiology of nicotine withdrawal symptoms. Importantly, these effects occur during nicotine withdrawal only and arise not from the combustible contents of cigarettes, but from the withdrawal from nicotine itself. This suggests that withdrawal from two of the current smoking cessation aids, varenicline and NRT, may also alter neuroinflammatory responses in the mesolimbic circuitry. Going forward, it will be important to evaluate the impact of these smoking cessation aids on microglia-related molecular and behavioral effects during nicotine withdrawal. Additional investigation into whether transcriptional reprogramming in microglia underlies these microglia-related effects or whether it is due to lack of nicotine stimulation during withdrawal will also advance our current understanding of cell-specific molecular mechanisms of nicotine withdrawal. These investigations may highlight potential microglial targets for therapeutic development of smoking cessation aids, in complement to existing ones. For instance, α7 nAChRs have been suggested as potential mediators of nicotine's inhibitory effect on microglial proinflammatory signals (*43*). Therefore, in-depth investigation of nicotine's directs effects on microglia may give rise to future therapeutic targets for suppression of microglial function during nicotine withdrawal. Long-term, further investigation into modulators of microglial function during nicotine withdrawal represents an untapped therapeutic avenue for smoking cessation.

MATERIALS AND METHODS

Animals

Male B6/129 F1 mice used for these studies were either purchased from the Jackson Laboratory (Bar Harbor, ME, USA; 8–10 weeks of age; 20–31 g) or bred in-house (8–10 weeks of age; 20–31 g). The B6/129 F1 mouse strain is a hybrid of C57BL/6 and 129SvEv strains that are commonly used for the development of knockout mouse models; therefore, information regarding nicotine response in a variety of behaviors in this strain is of value for future studies aimed at investigating underlying genetic mechanisms. All mice were housed in groups of two to four and randomly assigned to treatment conditions. They were maintained on a 12-hour light/12-hour dark cycle with food and water ad libitum in accordance with the University of South Carolina Animal Care and Use Committee. All behavioral testing sessions were conducted between 0900 and 1300 hours.

Osmotic drug delivery and treatment

(−)-Nicotine tartrate (MP Biomedicals, Solon, OH, USA) was dissolved in sterile 0.9% sodium chloride solution and then infused subcutaneously via osmotic minipumps (Alzet model 2002; DURECT Corporation, Cupertino, CA, USA) at a dose of 18 mg kg^{-1} day^{-1} for 15 days. Chronic treatment with nicotine at this dose yields a plasma level of approximately 0.3 μM in mice (reported as nicotine free base molecular weight), a concentration comparable to that observed in human smokers consuming an average of 17 cigarettes a day (plasma levels between 0.06 and 0.31 μM) (*64*). Furthermore, in vivo nicotine delivery in mice has shown this low-moderate dose to be the most effective in maintaining face validity with clinical withdrawal symptomology. Our past studies have used chronic nicotine doses ranging from 6 to 36 mg kg^{-1} day^{-1} (*11*–*15*), with the dose of 18 mg kg^{-1} day^{-1} being the lowest tested concentration able to elicit all the major hallmarks of nicotine withdrawal observed clinically (*5*–*10*). Control animals were implanted with osmotic minipumps containing only sterile 0.9% sodium chloride solution. Before the start of surgery, mice were anesthetized with isoflurane/oxygen mixture (1–3%), and minipumps were inserted using aseptic techniques. Surgical wounds were closed with 7-mm stainless steel wound clips (Reflex, Cellpoint Scientific, Gaithersburg, MD, USA), after which mice were left to recover on the recovery pad before they were returned to their individual cages. After 14 days of chronic administration of either saline or nicotine via osmotic minipumps, mice in the withdrawal groups (withdrawal from either nicotine or saline) were subjected to spontaneous withdrawal by the removal of their osmotic minipumps using a similar aseptic surgical approach as above. Animals in the chronic nicotine or chronic saline treatment groups underwent sham surgery, where an incision was made and restapled, without removal of the

pump. No molecular or behavioral differences were observed between the saline and saline withdrawal groups; therefore, these groups were combined during analysis.

Microglia depletion via chow treatment

Plexxikon Inc. (Berkeley, CA) provided the CSF1R inhibitor PLX5622, which was formulated in AIN-76A chow at a dose of 1200 parts per million by Research Diets (New Brunswick, NJ). Control chow was also provided. Male B6/129SF1 mice (8 weeks old) received either control chow or PLX5622 chow for 7 days before and throughout the withdrawal period. The selected dose and duration of PLX5622 treatment were based on previous studies showing between 80 and 90% microglial depletion with the same dose and treatment duration (*65*).

OF test and locomotor activity

The OF test is an anxiety-related behavioral model, which also allows simultaneous assay of overall locomotor activity levels in mice. All mice were tested in this model at the 24-hour withdrawal time point. Test chambers were wiped with 70% ethanol in between tests to remove any previous scent cues. The ethanol was allowed to dry completely before testing, and every testing session lasted for 15 min. For the analysis, Top Scan (Clever Sys Inc., Reston, VA, USA) software was used to track and evaluate mouse movement. Before tracking analysis for each mouse, a background profile was generated, and the testing chamber was calibrated in arena design mode according to the manufacturer's instructions. The center of the arena was defined as the central section making up 25% of the total area. Software output for each individual test includes total distance moved (in millimeters) and the time spent in the center quadrant (in percentage).

MB test

The MB test is an animal behavioral model of anxiety that has high predictive value in detecting anxiolytic drugs. All mice were tested in this model at the 48-hour withdrawal time point under low-light conditions. Mice were placed individually in small cages (29.0 cm × 17.5 cm), in which 20 marbles had been equally distributed on top of mouse bedding (5 cm deep). A lid was placed on top of the cage to prevent the mouse from jumping out of the cage during the test. Mice were left undisturbed for 15 min, after which the number of buried marbles (those covered by bedding three-quarters or more) was counted by an observer blinded to experimental conditions.

Quantitative PCR

Quantitative reverse-transcriptase PCR was performed as previously described (*66*) on caudate putamen or nucleus accumbens samples across all treatment groups. Briefly, RNA was isolated using the RNeasy Mini Kit (Qiagen, Venlo, the Netherlands), and qPCR reactions were assembled using synthesized complementary DNA and Thermo Scientific Maxima SYBR Green master mix along with 100 nM primers (Integrated DNA Technologies Inc., Coralville, IA, USA) diluted to 4.3 nM final concentration. The mRNA levels were determined using the $2^{-\Delta\Delta CT}$ method (*67*), and target genes were normalized to the housekeeping gene, hypoxanthine phosphoribosyltransferase. All gene expression values were normalized to their respective saline controls. Primer sequences are available upon request.

Protein carbonylation assay

Protein carbonyl derivatives were determined in caudate putamen and nucleus accumbens samples of all treatment groups using the OxiSelect Protein Carbonyl Immunoblot Kit (Cell Biolabs Inc., San Diego, CA, USA) following the manufacturer's details. Briefly, 20 μg of protein was resolved in Any kD mini-protean precast polyacrylamide gel (Bio-Rad Laboratories Inc., Hercules, CA, USA) and transferred to nitrocellulose membranes. Membranes were processed for 2,4-dinitrophenylhydrazine (DNPH) derivatization by equilibrating them in tris-buffered saline (TBS) containing 20% methanol, followed by washes in 2 N HCl, incubation in 1× DNPH, and final washes in 2 N HCl and 50% methanol. DNPH-treated membranes were then incubated with LI-COR blocking buffer (LI-COR, Lincoln, NE, USA) for 1 hour at room temperature before reacting overnight at 4°C with primary antibodies [anti-DNP (1:1000, Cell Biolabs Inc.) and GAPDH (1:1000, sc-32233, Santa Cruz Biotechnology, Santa Cruz, CA, USA)]. After washing in TBS–Tween 20, the blots were incubated with fluorescent secondary antibodies (1:20,000, LI-COR) in LI-COR blocking buffer for 1 hour at room temperature. Membranes were then washed, and immunolabeling detection and densitometry measurements were performed using the LICOR Odyssey System (LI-COR). DNP signals were normalized to GAPDH densities for each sample.

Immunohistochemistry and microglia morphological analysis

One brain hemisphere from each mouse was collected and fixed overnight in 4% paraformaldehyde in phosphate-buffered saline (PBS). Fixed brains were cryoprotected by leaving them overnight in 15% sucrose and then in 30% sucrose for 48 h. Cryoprotected brain hemispheres were sectioned through the striatum at 45 μm and processed for IBA1 immunohistochemistry. Briefly, cryosections were incubated in a rabbit anti-IBA1 primary antibody overnight (1:1000; Wako Catalog No. 019–19741), followed by a 2-hour incubation in a goat anti-rabbit secondary (1:500, Jackson ImmunoResearch Laboratories, West Grove, PA, USA). The signal was amplified with the avidin-biotin complex (Vector Labs) method (1:500) and visualized with Vector VIP peroxidase substrate to yield a purple reaction product. Images were generated at 200× magnification using a Leica DMI 3000B microscope (Leica Microsystems Inc., Buffalo Grove, IL, USA) fitted with a Leica DFC 290HD digital camera. Leica LAS core software was used for image acquisition. Morphological analyses were conducted with National Institutes of Health ImageJ software. For IBA1-positive cell count/density, cell area, and cell perimeter measurements, images were converted from RGB to 16-bit format before applying a threshold and subsequent binary mask. Objects within each masked image were then scanned, counted, and measured using the "Analyze Particles" command. Parameters for analysis of IBA1-positive cells were set in pixel units excluding any object under 400 ± 100 or above 4500 ± 1000 square pixel units. Objects positioned at the edge of the image field were excluded. For analysis of cell process count and length, primary processes extending directly from the cell body and no shorter than 5 μm in length were counted and measured. Five to six IBA1-positive cells per image field were analyzed for average process count and length measurements. For all morphological analyses, final measurements were reported in micrometers (resolution of 6.2 pixels per micrometer).

Isolation of nucleus accumbal microglia and astrocytes by MACS

Nucleus accumbal tissues (10 pooled animals per N) were diced with a sterile scalpel into small pieces in a sterile petri dish containing 2 ml of cold Hanks' balanced salt solution (minus Ca^{2+}, Mg^{2+}; Life

Technologies Corporation, Grand Island, NY, USA). This suspension was transferred into a 15-ml centrifuge tube and then spun at 300 *g* for 2 min at 4°C. Supernatant was discarded, and tissue was processed into single-cell suspension by enzyme dissociation using Miltenyi's adult brain dissociation kit (Miltenyi Biotec Inc., Auburn, CA, USA) according to the manufacturer's instructions. Following complete dissociation, cell suspension was applied to pre-wet MACS Smart Strainer (70 μm; Miltenyi Biotec Inc., Auburn, CA, USA), and the flow through was processed for microglia labeling with $CD11b^+$ microbeads (Miltenyi Biotec Inc., Auburn, CA, USA). Cells were washed with 2 ml of 0.5% bovine serum albumin (BSA) in PBS buffer and centrifuged at 300 *g* for 10 min at 4°C for removal of any unbounded beads from the pellet. Cell pellet was resuspended in 500 μl of 0.5% BSA in PBS buffer and then applied onto a prepped MACS MS column attached to an OctoMACS magnetic separator (Miltenyi Biotec Inc., Auburn, CA, USA). Flow through containing unlabeled cells was collected first, and $CD11b^+$ microglia were then collected by flushing out the magnetically labeled cells in the column into a microcentrifuge tube following the removal of the column from the magnetic separator. The flow through was immediately processed for astrocyte labeling using the Anti–ACSA-2 MicroBead Kit (Miltenyi Biotec Inc., Auburn, CA, USA) according to the manufacturer's instructions. In a similar way to the magnetic separation step in $CD11b^+$ microglia isolation, $ACSA\text{-}2^+$ astrocytes were also purified and collected.

Behavioral and molecular data analyses

Results are presented as mean ± SEM. For behavioral data, statistical differences between groups were determined using two-way analysis of variance (ANOVA) followed by the multiple two-stage linear step-up procedure of Benjamini, Krieger, and Yekutieli multiple comparisons test. For molecular data, statistical differences between groups were determined using either one-way or two-way ANOVA followed by Bonferroni's or Tukey's honestly significant difference (HSD) multiple comparison test. All statistical analyses were done in GraphPad Prism 8.0 (GraphPad Software, La Jolla, CA, USA). Statistical tests used for each set of experiments and their results are presented in Table S1.

SUPPLEMENTARY MATERIALS

Supplementary material for this article is available at http://advances.sciencemag.org/cgi/content/full/5/10/eaax7031/DC1

Table S1. Statistical tests used for each set of experiments and test results.

REFERENCES AND NOTES

1. J. M. Samet, Tobacco smoking: The leading cause of preventable disease worldwide. *Thorac. Surg. Clin.* **23**, 103–112 (2013).
2. M. A. Babizhayev, The detox strategy in smoking comprising nutraceutical formulas of non-hydrolyzed carnosine or carcinine used to protect human health. *Hum. Exp. Toxicol.* **33**, 284–316 (2013).
3. R. Polosa, N. L. Benowitz, Treatment of nicotine addiction: Present therapeutic options and pipeline developments. *Trends Pharmacol. Sci.* **32**, 281–289 (2011).
4. World Health Organization, *WHO Global Report: Mortality Attributable to Tobacco. Geneva, Switzerland* (2012); http://apps.who.int/iris/bitstream/10665/44815/1/9789241564434_eng.pdf.
5. J. W. Coe, P. R. Brooks, M. G. Vetelino, M. C. Wirtz, E. P. Arnold, J. Huang, S. B. Sands, T. I. Davis, L. A. Lebel, C. B. Fox, A. Shrikhande, J. H. Heym, E. Schaeffer, H. Rollema, Y. Lu, R. S. Mansbach, L. K. Chambers, C. C. Rovetti, D. W. Schulz, F. D. Tingley, B. T. O'Neill, Varenicline: An α4β2 nicotinic receptor partial agonist for smoking cessation. *J. Med. Chem.* **48**, 3474–3477 (2005).
6. H. Rollema, L. K. Chambers, J. W. Coe, J. Glowa, R. S. Hurst, L. A. Lebel, Y. Lu, R. S. Mansbach, R. J. Mather, C. C. Rovetti, S. B. Sands, E. Schaeffer, D. W. Schulz, F. D. Tingley III, K. E. Williams, Pharmacological profile of the α4β2 nicotinic acetylcholine receptor partial agonist varenicline, an effective smoking cessation aid. *Neuropharmacology* **52**, 985–994 (2007).
7. Y. Xiao, H. Fan, J. L. Musachio, Z.-L. Wei, S. K. Chellappan, A. P. Kozikowski, K. J. Kellar, Sazetidine-A, a novel ligand that desensitizes α4β2 nicotinic acetylcholine receptors without activating them. *Mol. Pharmacol.* **70**, 1454–1460 (2006).
8. M. W. Salter, B. Stevens, Microglia emerge as central players in brain disease. *Nat. Med.* **23**, 1018–1027 (2017).
9. A. Miyamoto, H. Wake, A. W. Ishikawa, K. Eto, K. Shibata, H. Murakoshi, S. Koizumi, A. J. Moorhouse, Y. Yoshimura, J. Nabekura, Microglia contact induces synapse formation in developing somatosensory cortex. *Nat. Commun.* **7**, 12540 (2016).
10. L. Weinhard, G. di Bartolomei, G. Bolasco, P. Machado, N. L. Schieber, U. Neniskyte, M. Exiga, A. Vadisiute, A. Raggioli, A. Schertel, Y. Schwab, C. T. Gross, Microglia remodel synapses by presynaptic trogocytosis and spine head filopodia induction. *Nat. Commun.* **9**, 1228 (2018).
11. L. Torres, J. Danver, K. Ji, J. T. Miyauchi, D. Chen, M. E. Anderson, B. L. West, J. K. Robinson, S. E. Tsirka, Dynamic microglial modulation of spatial learning and social behavior. *Brain Behav. Immun.* **55**, 6–16 (2016).
12. M. M. Torregrossa, P. R. Corlett, J. R. Taylor, Aberrant learning and memory in addiction. *Neurobiol. Learn. Mem.* **96**, 609–623 (2011).
13. M. G. Kutlu, T. J. Gould, Effects of drugs of abuse on hippocampal plasticity and hippocampus-dependent learning and memory: Contributions to development and maintenance of addiction. *Learn. Mem.* **23**, 515–533 (2016).
14. M. E. Lull, M. L. Block, Microglial activation and chronic neurodegeneration. *Neurotherapeutics* **7**, 354–365 (2010).
15. M. Schieber, N. S. Chandel, ROS function in redox signaling and oxidative stress. *Curr. Biol.* **24**, R453–R462 (2014).
16. J.-S. Seo, J.-Y. Park, J. Choi, T.-K. Kim, J.-H. Shin, J.-K. Lee, P.-L. Han, NADPH oxidase mediates depressive behavior induced by chronic stress in mice. *J. Neurosci.* **32**, 9690–9699 (2012).
17. G. Li, J. Gong, H. Lei, J. Liu, X. Z. S. Xu, Promotion of behavior and neuronal function by reactive oxygen species in C. elegans. *Nat. Commun.* **7**, 13234 (2016).
18. M. Ikawa, H. Okazawa, T. Kudo, M. Kuriyama, Y. Fujibayashi, M. Yoneda, Evaluation of striatal oxidative stress in patients with Parkinson's disease using [62Cu]ATSM PET. *Nucl. Med. Biol.* **38**, 945–951 (2011).
19. L. M. Yager, A. F. Garcia, A. M. Wunsch, S. M. Ferguson, The ins and outs of the striatum: Role in drug addiction. *Neuroscience* **301**, 529–541 (2015).
20. J. R. Turner, R. Ray, B. Lee, L. Everett, J. Xiang, C. Jepson, K. H. Kaestner, C. Lerman, J. A. Blendy, Evidence from mouse and man for a role of neuregulin 3 in nicotine dependence. *Mol. Psychiatry* **19**, 801–810 (2014).
21. M. L. Fisher, R. M. LeMalefant, L. Zhou, G. Huang, J. R. Turner, Distinct roles of CREB within the ventral and dorsal hippocampus in mediating nicotine withdrawal phenotypes. *Neuropsychopharmacology* **42**, 1599–1609 (2017).
22. A. C. Manhães, M. C. Guthierrez, C. C. Filgueiras, Y. Abreu-Villaça, Anxiety-like behavior during nicotine withdrawal predict subsequent nicotine consumption in adolescent C57BL/6 mice. *Behav. Brain Res.* **193**, 216–224 (2008).
23. M. E. Piper, J. W. Cook, T. R. Schlam, D. E. Jorenby, T. B. Baker, Anxiety diagnoses in smokers seeking cessation treatment: Relations with tobacco dependence, withdrawal, outcome and response to treatment outcome and response to treatment. *Addiction* **106**, 418–427 (2011).
24. L. Levita, R. Hoskin, S. Champi, Avoidance of harm and anxiety: A role for the nucleus accumbens. *Neuroimage* **62**, 189–198 (2012).
25. S. J. Russo, E. J. Nestler, The brain reward circuitry in mood disorders. *Nat. Rev. Neurosci.* **14**, 609–625 (2013).
26. S. Salim, N. Sarraj, M. Taneja, K. Saha, M. V. Tejada-Simon, G.Chugh, Moderate treadmill exercise prevents oxidative stress-induced anxiety-like behavior in rats. *Behav. Brain Res.* **208**, 545–552 (2010).
27. G. Patki, N. Solanki, F. Atrooz, F. Allam, S. Salim, Depression, anxiety-like behavior and memory impairment are associated with increased oxidative stress and inflammation in a rat model of social stress. *Brain Res.* **1539**, 73–86 (2013).
28. D. Boche, V. H. Perry, J. A. R. Nicoll, Review: Activation patterns of microglia and their identification in the human brain. *Neuropathol. Appl. Neurobiol.* **39**, 3–18 (2013).
29. X. Ding, M. Zhang, R. Gu, G. Xu, H. Wu, Activated microglia induce the production of reactive oxygen species and promote apoptosis of co-cultured retinal microvascular pericytes. *Graefes Arch. Clin. Exp. Ophthalmol.* **255**, 777–788 (2017).
30. Y. J. Suzuki, M. Carini, D. A. Butterfield, Protein carbonylation. *Antioxid. Redox Signal* **12**, 323–325 (2010).
31. K. Sidiropoulos, G. Viteri, C. Sevilla, S. Jupe, M. Webber, M. Orlic-Milacic, B. Jassal, B. May, V. Shamovsky, C. Duenas, K. Rothfels, L. Matthews, H. Song, L. Stein, R. Haw, P. D'Eustachio, P. Ping, H. Hermjakob, A. Fabregat, Reactome enhanced pathway visualization. *Bioinformatics* **33**, 3461–3467 (2017).
32. A. Orient, A. Donkó, A. Szabó, T. L. Leto, M. Geiszt, Novel sources of reactive oxygen species in the human body. *Nephrol. Dial. Transplant.* **22**, 1281–1288 (2007).
33. R. Rastogi, X. Geng, F. Li, Y. Ding, NOX activation by subunit interaction and underlying mechanisms in disease. *Front. Cell. Neurosci.* **10**, 301 (2016).
34. H. Blaser, C. Dostert, T. W. Mak, D. Brenner, TNF and ROS crosstalk in inflammation. *Trends Cell Biol.* **26**, 249–261 (2016).

35. Y. S. Kim, M. J. Morgan, S. Choksi, Z. G. Liu, TNF-induced activation of the Nox1 NADPH oxidase and its role in the induction of necrotic cell death. *Mol. Cell* **26**, 675–687 (2007).
36. J. L. Miller, K. Velmurugan, M. J. Cowan, V. Briken, The type I NADH dehydrogenase of *Mycobacterium tuberculosis* counters phagosomal NOX2 activity to inhibit TNF-α-mediated host cell apoptosis. *PLOS Pathog.* **6**, e1000864 (2010).
37. T. R. Guilarte, M. K. Loth, S. R. Guariglia, TSPO finds NOX2 in microglia for redox homeostasis. *Trends Pharmacol. Sci.* **37**, 334–343 (2016).
38. Z. Nayernia, V. Jaquet, K.-H. Krause, New insights on NOX enzymes in the central nervous system. *Antioxid. Redox Signal* **20**, 2815–2837 (2014).
39. M. Prinz, J. Priller, Tickets to the brain: Role of CCR2 and CX3CR1 in myeloid cell entry in the CNS. *J. Neuroimmunol.* **224**, 80–84 (2010).
40. M. Mizutani, P. A. Pino, N. Saederup, I. F. Charo, R. M. Ransohoff, A. E. Cardona, The fractalkine receptor but not CCR2 is present on microglia from embryonic development throughout adulthood. *J. Immunol.* **188**, 29–36 (2011).
41. A. L. Brody, R. Hubert, R. Enoki, L. Y. Garcia, M. S. Mamoun, K. Okita, E. D. London, E. L. Nurmi, L. C. Seaman, M. A. Mandelkern, Effect of cigarette smoking on a marker for neuroinflammation: A [^{11}C]DAA1106 positron emission tomography study. *Neuropsychopharmacology* **42**, 1630–1639 (2017).
42. L. M. De Biase, K. E. Schuebel, Z. H. Fusfeld, K. Jair, I. A. Hawes, R. Cimbro, H.-Y. Zhang, Q.-R. Liu, H. Shen, Z.-X. Xi, D. Goldman, A. Bonci, Local cues establish and maintain region-specific phenotypes of basal ganglia microglia. *Neuron* **95**, 341–356 (2017).
43. M. Noda, A. I. Kobayashi, Nicotine inhibits activation of microglial proton currents via interactions with α7 acetylcholine receptors. *J. Physiol. Sci.* **67**, 235–245 (2017).
44. G. Villafane, P. Cesaro, A. Rialland, S. Baloul, S. Azimi, C. Bourdet, J. le Houezec, I. Macquin-Mavier, P. Maison, Chronic high dose transdermal nicotine in Parkinson's disease: An open trial. *Eur. J. Neurol.* **14**, 1313–1316 (2007).
45. P. Newhouse, K. Kellar, P. Aisen, H. White, K. Wesnes, E. Coderre, A. Pfaff, H. Wilkins, D. Howard, E. D. Levin, Nicotine treatment of mild cognitive impairment: A 6-month double-blind pilot clinical trial. *Neurology* **78**, 91–101 (2012).
46. N. L. Benowitz, Nicotine addiction. *N. Engl. J. Med.* **362**, 2295–2303 (2010).
47. J. K. Brynildsen, J. Najar, L.-M. Hsu, D. B. Vaupel, H. Lu, T. J. Ross, Y. Yang, E. A. Stein, A novel method to induce nicotine dependence by intermittent drug delivery using osmotic minipumps. *Pharmacol. Biochem. Behav.* **142**, 79–84 (2016).
48. S. Semenova, X. Jin, T. D. McClure-Begley, M. P. Tadman, M. J. Marks, A. Markou, Differential effects of withdrawal from intermittent and continuous nicotine exposure on reward deficit and somatic aspects of nicotine withdrawal and expression of α4β2* nAChRs in Wistar male rats. *Pharmacol. Biochem. Behav.* **171**, 54–65 (2018).
49. G. M. Lewitus, S. C. Konefal, A. D. Greenhalgh, H. Pribiag, K. Augereau, D. Stellwagen, Microglial TNF-α suppresses cocaine-induced plasticity and behavioral sensitization. *Neuron* **90**, 483–491 (2016).
50. J. M. Schwarz, S. D. Bilbo, Adolescent morphine exposure affects long-term microglial function and later-life relapse liability in a model of addiction. *J. Neurosci.* **33**, 961–971 (2013).
51. J. W. VanRyzin, L. A. Pickett, M. M. McCarthy, Microglia: Driving critical periods and sexual differentiation of the brain. *Dev. Neurobiol.* **78**, 580–592 (2018).
52. A. Panday, M. K. Sahoo, D. Osorio, S. Batra, NADPH oxidases: An overview from structure to innate immunity-associated pathologies. *Cell. Mol. Immunol.* **12**, 5–23 (2015).
53. M. W. Ma, J. Wang, Q. Zhang, R. Wang, K. M. Dhandapani, R. K. Vadlamudi, D. W. Brann, NADPH oxidase in brain injury and neurodegenerative disorders. *Mol. Neurodegener.* **12**, 7 (2017).
54. Y. Huo, P. Rangarajan, E. A. Ling, S. T. Dheen, Dexamethasone inhibits the Nox-dependent ROS production via suppression of MKP-1-dependent MAPK pathways in activated microglia. *BMC Neurosci.* **12**, 49 (2011).
55. D. J. Stein, M. F. Vasconcelos, L. Albrechet-Souza, K. M. M. Ceresér, R. M. M. de Almeida, Microglial over-activation by social defeat stress contributes to anxiety- and depressive-like behaviors. *Front. Behav. Neurosci.* **11**, 207 (2017).
56. Y.-L. Wang, Q.-Q. Han, W.-Q. Gong, D.-H. Pan, L.-Z. Wang, W. Hu, M. Yang, B. Li, J. Yu, Q. Liu, Microglial activation mediates chronic mild stress-induced depressive- and anxiety-like behavior in adult rats. *J. Neuroinflammation* **15**, 21 (2018).
57. E. Choleris, A. W. Thomas, M. Kavaliers, F. S. Prato, A detailed ethological analysis of the mouse open field test: Effects of diazepam, chlordiazepoxide and an extremely low frequency pulsed magnetic field. *Neurosci. Biobehav. Rev.* **25**, 235–260 (2001).
58. L. B. Nicolas, Y. Kolb, E. P. Prinssen, A combined marble burying–locomotor activity test in mice: A practical screening test with sensitivity to different classes of anxiolytics and antidepressants. *Eur. J. Pharmacol.* **547**, 106–115 (2006).
59. R. Saravia, M. Ten-Blanco, M. T. Grande, R. Maldonado, F. Berrendero, Anti-inflammatory agents for smoking cessation? Focus on cognitive deficits associated with nicotine withdrawal in male mice. *Brain Behav. Immun.* **75**, 228–239 (2019).
60. E. D. Levin, M. Castonguay, G. D. Ellison, Effects of the nicotinic receptor blocker mecamylamine on radial-arm maze performance in rats. *Behav. Neural Biol.* **48**, 206–212 (1987).
61. S. N. Katner, S. A. Davis, A. J. Kirsten, M. A. Taffe, Effects of nicotine and mecamylamine on cognition in rhesus monkeys. *Psychopharmacology* **175**, 225–240 (2004).
62. A. C. Baakman, R. Alvarez-Jimenez, R. Rissmann, E. S. Klaassen, J. Stevens, S. C. Goulooze, J. C. G. den Burger, E. L. Swart, J. M. A. van Gerven, G. J. Groeneveld, An anti-nicotinic cognitive challenge model using mecamylamine in comparison with the anti-muscarinic cognitive challenge using scopolamine. *Br. J. Clin. Pharmacol.* **83**, 1676–1687 (2017).
63. D. Gonzales, S. I. Rennard, M. Nides, C. Oncken, S. Azoulay, C. B. Billing, E. J. Watsky, J. Gong, K. E. Williams, K. R. Reeves; Varenicline Phase 3 Study Group, Varenicline, an α4β2 nicotinic acetylcholine receptor partial agonist, vs sustained-release bupropion and placebo for smoking cessation: A randomized controlled trial. *JAMA* **296**, 47–55 (2006).
64. S. G. Matta, D. J. Balfour, N. L. Benowitz, R. T. Boyd, J. J. Buccafusco, A. R. Caggiula, C. R. Craig, A. C. Collins, M. I. Damaj, E. C. Donny, P. S. Gardiner, S. R. Grady, U. Heberlein, S. S. Leonard, E. D. Levin, R. J. Lukas, A. Markou, M. J. Marks, S. E. McCallum, N. Parameswaran, K. A. Perkins, M. R. Picciotto, M. Quik, J. E. Rose, A. Rothenfluh, W. R. Schafer, I. P. Stolerman, R. F. Tyndale, J. M. Wehner, J. M. Zirger, Guidelines on nicotine dose selection for in vivo research. *Psychopharmacology* **190**, 269–319 (2007).
65. J. Han, R. A. Harris, X.-M. Zhang, An updated assessment of microglia depletion: Current concepts and future directions. *Mol. Brain* **10**, 25 (2017).
66. J. N. Cleck, L. E. Ecke, J. A. Blendy, Endocrine and gene expression changes following forced swim stress exposure during cocaine abstinence in mice. *Psychopharmacology* **201**, 15–28 (2008).
67. K. J. Livak, T. D. Schmittgen, Analysis of relative gene expression data using real-time quantitative PCR and the $2^{-\Delta\Delta C}_{T}$ method. *Methods* **25**, 402–408 (2001).

Acknowledgments: We thank Plexxikon Inc. for providing the CSF1R inhibitor PLX5622. **Funding:** This work was supported by the National Institutes of Health–National Institute on Drug Abuse grants DA044311 and DA032681 to J.R.T., grants DA031747 and DA041513 to P.I.O., the NIDA T32 DA016176 (R.D.C.), and a Research Starter Grant from the PhRMA foundation to J.R.T. **Author contributions:** The experiment was designed by A.A. and J.R.T. Animal surgeries and minipump implantation for saline and nicotine delivery as well as PLX5622 treatment were carried out by A.A. Brain sectioning was performed by A.A. and L.G. Immunohistochemistry (IHC) was carried out by L.R.F. Imaging of IHC slides and generation of IHC figures for publication were carried out by A.A., S.W.D., and J.R.T. ImageJ analysis for IHC data was performed by A.G. and P.I.O. Other molecular experiments were performed by A.A., L.G., R.D.C., M.D.W., and S.S.L.C. Behavioral experiments were performed by A.A. and M.L.F. Data analyses were performed by A.A. Manuscript was written by A.A. and J.R.T. All authors provided critical feedback on the manuscript and contributed substantially to and approved the final version of the manuscript. **Competing interests:** The authors declare that they have no competing interests. **Data and materials availability:** All data needed to evaluate the conclusions in the paper are present in the paper and/or the Supplementary Materials. Additional data related to this paper may be requested from the authors. PLX-5622 can be provided by Plexxikon pending scientific review and a completed material transfer agreement. Requests for this compound should be submitted to P. Singh at Plexxikon Inc. (psingh@plexxikon.com).

Submitted 15 April 2019
Accepted 14 September 2019
Published 9 October 2019
10.1126/sciadv.aax7031

Citation: A. Adeluyi, L. Guerin, M. L. Fisher, A. Galloway, R. D. Cole, S. S. L. Chan, M. D. Wyatt, S. W. Davis, L. R. Freeman, P. I. Ortinski, J. R. Turner, Microglia morphology and proinflammatory signaling in the nucleus accumbens during nicotine withdrawal. *Sci. Adv.* **5**, eaax7031 (2019).